Journal of The Electrochemical Society, **158** (5) H530-H535 (2011)
0013-4651/2011/158(5)/H530/6/$28.00 © The Electrochemical Society

Growth and Characterization of AlN and AlGaN Epitaxial Films on AlN Single Crystal Substrates

R. Dalmau,[a,z] B. Moody,[a] R. Schlesser,[a] S. Mita,[a] J. Xie,[a] M. Feneberg,[b] B. Neuschl,[b] K. Thonke,[b] R. Collazo,[c] A. Rice,[c] J. Tweedie,[c] and Z. Sitar[c]

[a]*HexaTech Inc., Morrisville, North Carolina 27560, USA*
[b]*Institut für Quantenmaterie/Gruppe Halbleiterphysik, Universität Ulm, Ulm 89069, Germany*
[c]*Department of Materials Science and Engineering, North Carolina State University, Raleigh, North Carolina 27695, USA*

AlN and AlGaN epitaxial films were deposited by metal organic chemical vapor deposition on single crystal AlN substrates processed from AlN boules grown by physical vapor transport. Structural, chemical, and optical characterization demonstrated the high crystalline quality of the films and interfaces.
 [DOI: 10.1149/1.3560527]

Manuscript submitted October 28, 2010; revised manuscript received December 14, 2010. Published March 21, 2011. This was Paper 1761 presented at the Las Vegas, Nevada, Meeting of the Society, October 10-15, 2010.

AlN and high Al content AlGaN alloys are being actively pursued for applications ranging from deep UV light emitting diodes to high-power electronic devices. Emitters down to 210 nm have been demonstrated,[1] however, the efficiencies remain low. The AlN and AlGaN active layers of these devices have primarily been grown on foreign substrates, such as sapphire and silicon carbide. The density of threading dislocations in nitride films grown on foreign substrates is high, typically $>10^8$ cm^{-2} even when special growth techniques are employed, and represents a major obstacle to improved device performance. Recently, AlN single crystals with significantly lower dislocation density ($<10^4$ cm^{-2}) and in sizes suitable for device research have been developed as native substrates for nitride epitaxy.[2] AlN single crystal substrates are ideal for growth of AlN and Al-rich AlGaN films with low densities of extended defects and non-radiative recombination centers, resulting in higher internal quantum efficiency.

As these native substrates became available, studies on AlN homoepitaxy[3–8] and AlGaN heteroepitaxy[9,10] have been reported. AlN possesses high hardness and chemical stability, and forms a stable native hydroxide surface layer upon exposure to ambient air or water,[11] necessitating the development of proper surface polishing and preparation processes in order to enable high quality epitaxy. Nikishin et al.[5] grew AlN/$Al_{0.08}Ga_{0.92}N$ short-period superlattices on AlN substrates and attributed the higher dislocation density observed in the superlattices to incomplete oxide removal, performed under ammonia nitridation conditions at 800°C, prior to epitaxy. In other studies, AlN films were grown on substrates showing remnant surface scratches after chemo-mechanical polishing (CMP), evidence of incomplete removal of residual work damage.[8] Improved surface processing will be critical for achieving high quality epitaxy on AlN. Furthermore, studies of strain relaxation in AlGaN alloys grown on AlN are necessary to guide device design and ensure low defect densities are preserved in heterostructure active layers. Grandusky et al.[10] reported that pseudomorphic n-type $Al_{0.6}Ga_{0.4}N$ layers up to 0.5 μm thick may be grown on AlN.

In this study, AlN and AlGaN epitaxial films were deposited on AlN substrates by metal organic chemical vapor deposition (MOCVD) and characterized by high resolution x-ray diffraction (HRXRD), secondary ion mass spectrometry (SIMS), photoluminescence (PL) spectroscopy, atomic force microscopy (AFM), and scanning transmission electron microscopy (STEM).

Experimental

The *c*-plane, Al-polar, epi-ready AlN substrates used in this study were processed from AlN boules grown by physical vapor transport (PVT) and were oriented within 2° of (00.1), unless otherwise noted. Further details of the AlN boule growth have been published elsewhere.[12,13] Substrates were sliced from boules using a diamond wire saw and subsequently lapped and mechanically polished using decreasing abrasive sizes in order to remove the plastically damaged subsurface layer caused by slicing. Epi-ready surfaces, free of remnant subsurface damage from mechanical polishing, were obtained by a final CMP step in a proprietary alkaline slurry of sub-micron sized abrasives. Prior to epitaxy, as-polished substrates were ultrasonically cleaned in organic solvents and wet etched in a 3:1 solution of sulfuric and phosphoric acids for 10 min at 90°C. Wet etched substrates were then rinsed and dried, and transferred into a vertical, cold-walled, rf-heated, low-pressure MOCVD reactor. The reactor was back-filled with ammonia and substrates were ramped within 5 min to a temperature of 1250°C under flowing ammonia, at which point they were annealed at 1250°C and 60 Torr for an additional 15 min, in order to nitride the AlN surface hydroxide and provide a surface suitable for epitaxy. More details on the AlN substrate surface preparation and chemistry can be found in Ref. 14. AlN epitaxial layers were deposited using trimethylaluminum (TMA) and ammonia as the aluminum and nitrogen precursors, respectively, at 1100–1250°C under 20 Torr total pressure, with V/III ratios of 180–300 in either N_2 or H_2 diluent. AlGaN films of different compositions were grown at a temperature of 1100°C by first depositing an AlN homoepitaxial layer (200 nm thick, except where otherwise noted) and then introducing the gallium precursor into the above-described gas flow.

HRXRD was performed on a Philips X'Pert Materials Research Diffractometer using Cu $K\alpha$ radiation. Double axis rocking curves (RCs) were obtained with a four-bounce Ge [220] monochromator on the incident beam side and an open detector. On-axis RCs were recorded from the symmetric (00.2) reflection, while off-axis RCs were recorded from the skew-symmetric (10.2) reflection. In addition, triple axis ω-2θ (2θ-ω) scans and reciprocal space maps (RSMs) were obtained with a three-bounce Ge analyzer crystal in front of the detector. Calibrated SIMS depth profiling was performed using a CAMECA IMS-6f with 50 nA Cs^+ beam. PL was excited by a pulsed ArF excimer laser (λ= 193 nm). The samples were placed within a variable temperature cryostat, allowing for measurements between liquid helium temperature and room temperature. PL emission was analyzed by a high resolution grating monochromator with 2400 grooves/mm, and recorded by a charge coupled device camera. The grating was used in second order, leading to a spectral resolution better than 3×10^{-3} nm, corresponding to ~100 μeV at 6 eV. Surface morphology was characterized by AFM using a JEOL JSPM-5200 in tapping mode. Electron-transparent foils, ~140 nm thick, were prepared for STEM analysis using a focused ion beam (FIB) with a Ga^+ primary beam. Carbon (C) and Platinum (Pt) layers were applied to the film surface prior to FIB processing. STEM imaging was performed in a Hitachi HD-2300

[z] E-mail: rdalmau@hexatechinc.com

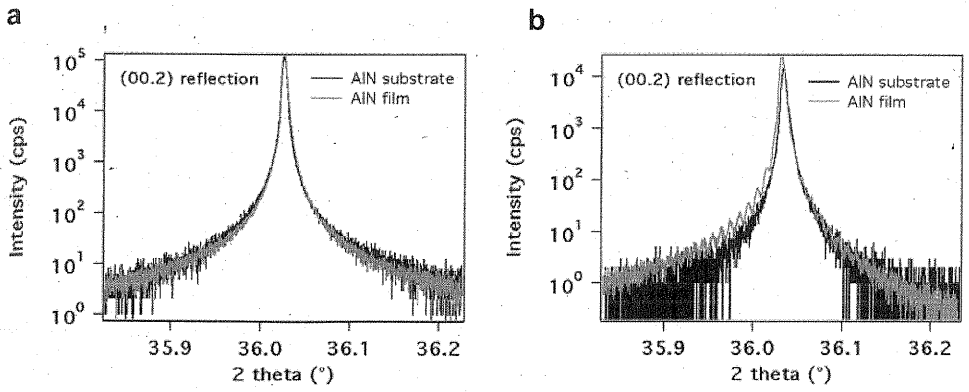

Figure 1. HRXRD triple axis 2θ-ω scans of AlN bulk substrates after CMP and after deposition of AlN homoepitaxial films grown at (a) 1100°C and (b) 1250°C. The FWHM of the (00.2) Bragg peaks is ~18 arcsec.

operated at 200 kV and equipped with a high angle annular dark field (HAADF) detector for elemental contrast (Z-contrast) imaging.

Results and Discussion

AlN homoepitaxy.— AlN substrate processing was critical for obtaining epitaxial films that maintained the crystalline quality of the substrates. Typical RC widths of AlN substrates were 12–40 arcsec for the (00.2) reflection and 12–60 arcsec for the (10.2) reflection, demonstrating excellent crystalline quality. The RCs were mostly symmetric and single-peaked, but occasionally additional, low-intensity sub-peaks were observed on the main peak shoulders, indicating the presence of low-angle grain boundaries (LAGB) in some of the substrates. Films deposited on mechanically damaged or improperly-prepared substrate surfaces were characterized by rough surfaces, grain nucleation on scratches, cracks, and asymmetric shoulders in triple axis 2θ-ω scans, indicating the films were strained due to re-nucleation and grain coalescence on these surfaces.[14] In contrast, films deposited on substrates processed by CMP and in-situ nitridation were smooth and crack-free. HRXRD analysis indicated the films reproduced the crystalline structure of the substrates. Figure 1a shows the triple axis 2θ-ω scans of the (00.2) reflection, which are highly sensitive to lattice dilation and probed the top 40 μm of the samples, from an AlN substrate prior to epitaxy and after deposition of an AlN homoepitaxial film grown at 1100°C. The lack of any peak shifts or shoulders in the film scan indicated that the film was epitaxial and strain-free.

Figure 1b shows the same scans from a homoepitaxial AlN film grown at 1250°C. The film scan again overlies the substrate scan very closely. However, new features, in the form of oscillations in the film scan, are observed. The film thickness calculated from the fringe spacing using the following expression

$$T = \lambda/(2\Delta\theta\cos\theta) \quad [1]$$

where T is the film thickness, $\Delta\theta$ is the fringe spacing, and θ is the Bragg angle, was ~1 μm. However, the calibrated film growth rate and film thickness measurements by other methods indicated the film thickness was ~1.2 μm. The reason for this discrepancy will be discussed below, together with SIMS results of the homoepitaxial films. Thickness fringes of this type are commonly observed in semiconductor heterostructures and are an indicator of abrupt, high-quality interfaces.

These films were analyzed by calibrated SIMS in order to quantitatively determine the concentrations of C, O, and Si impurities in the films and underlying bulk substrates. The results of SIMS depth profiling are shown in Fig. 2, which correspond to the samples whose HRXRD scans are shown in Fig. 1. SIMS analysis indicated that the concentrations of major impurities were significantly lower in the homoepitaxial films than in the bulk substrates. These differences can be attributed to the much lower growth temperature for MOCVD (~1100–1250°C) versus PVT bulk crystal growth (~2200°C), and the higher purity of precursor materials used in MOCVD (TMA, NH_3) versus PVT (AlN powder, N_2). The largest difference was observed in the Si impurity concentration, which varied ~2–3 orders of magnitude, while C and O concentrations varied about 1 order of magnitude, as shown in Table I and Fig. 2. This difference in Si impurity incorporation, and the corresponding electronic density variation, may account for the thickness fringes observed in HRXRD. The reason fringes are not observed in some samples may be due to differences in growth temperature, yielding differing impurity profiles, especially for Si. Note that the variation in Si concentration is much more abrupt in Fig. 2b than Fig. 2a. Thus, the film thickness obtained from HRXRD measurement of this sample, as mentioned above, corresponded to ~1 μm, roughly the position where the Si impurity profile begins to decrease, instead of ~1.2 μm, the depth of the film/substrate interface. It is reasonable to assume that a lower impurity concentration in homoepitaxial films implies that these films also contain lower concentrations of

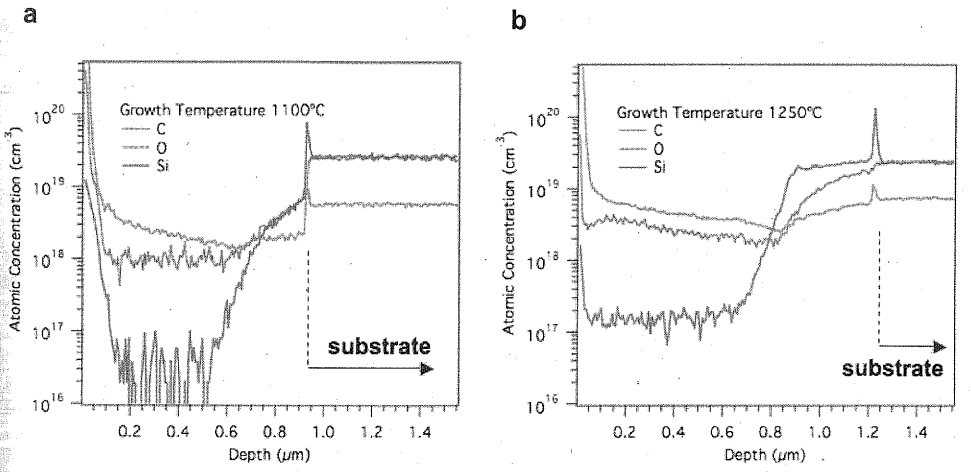

Figure 2. (Color online) Calibrated SIMS depth profiles for C, O, Si impurities in homoepitaxial AlN films grown at (a) 1100°C and (b) 1250°C.

Table I. Impurity concentrations in AlN (cm^{-3}) derived from calibrated SIMS depth profiles.

	[C]	[O]	[Si]
AlN film, 1100°C growth	1×10^{18}	2×10^{18}	$< 1 \times 10^{17}$
AlN film, 1250°C growth	3×10^{18}	6×10^{18}	2×10^{17}
AlN substrate average	3×10^{19}	1×10^{19}	3×10^{19}

compensating defects, which will be critical for successful doping of AlN and high-Al content AlGaN.

Low temperature (8 K) PL spectra of these two homoepitaxial films show a rich fine structure of excitonic contributions below the band gap, Fig. 3. Besides the *A* free exciton (X_{A1}) transition at 6.0414 eV, donor bound excitonic transitions ($D_n{}^{\circ}X_A$, n = 1, 2, 3) were observed at 6.0127, 6.0190, and 6.0280 eV. Their full-width at half-maximum was determined to be 450 μeV after Lorentzian fitting. This extremely small linewidth was attributed to the growth of homoepitaxial films which possessed low concentrations of impurities and were free of the misfit strain observed in heteroepitaxy on non-native substrates. The excited state of the *A* free exciton was visible in the film grown at 1100°C, after magnification, at 6.0807 eV (not shown). The energetic spacing between the ground state and the first excited state transitions of the *A* exciton allowed a calculation, assuming a hydrogenic model, of the exciton binding energy, which yielded 52.4 meV, a value similar to previous reports for heteroepitaxial AlN films grown by MOCVD.[15,16] Based on this, the fundamental band gap of homoepitaxial AlN was determined to be 6.094 eV at T = 8 K, consistent with a value of 6.096 eV for unstrained bulk AlN at T = 1.7 K, reported in Ref. 17.

Figure 4 shows AFM images of as-grown films deposited on nominally on-axis wafers. The topographs show uniform terraces with step heights of ~1 nm and terrace widths of ~500 nm. AFM images (not shown) of homoepitaxial films grown on substrates oriented up to 13° off-axis from (00.1) indicated that the terrace width increased as the substrate orientation approached the *c*-plane, as expected from geometrical considerations. As shown in Fig. 4b, micro-steps with a height of ~2.5 Å were also observed, corresponding to the bilayer height of (00.1)-oriented AlN, suggesting that the terraces of ~500 nm width were the result of a micro-step bunching phenomenon. The wide terraces of nominally on-axis films, as in Fig. 4a, were characterized by small, randomly located protrusions of ~1 nm height with an area density of ~10^9 cm^{-2}. These are thought to be caused by the gradual formation of a native surface hydroxide due to hydrolysis upon ambient air exposure, as the size and area density of the protrusions increased with increasing duration of exposure to ambient air.[14] Hexagonal pits ~600 nm wide are also seen in Fig. 4a. The white band to the right of the pits is an AFM scanning artifact associated with the large vertical scale change. It was observed that the size of the hexagonal pits increased with increasing film thickness. The mean pit width was found to be 400, 600, and 800 nm for 1, 2, and 3 μm thick films, respectively. Pits in films grown on off-axis oriented substrates were slightly elongated in one direction due to the lattice plane tilt. Pits in on-axis films exhibited an inverted hexagonal pyramid morphology with sidewalls inclined at ~30° relative to the sample normal. This angle roughly corresponds to the inclination angle of the low index {10.1} planes of the AlN wurtzite lattice. The site density of hexagonal pits was highly non-uniform over the films' surface, varying from $< 10^4$ cm^{-3} over most of the films' surface to $> 10^6$ cm^{-3} in some localized regions, and appeared to depend on the microstructure of the underlying AlN substrate. The pit density was greatest in regions of the films corresponding to regions of the substrates containing LAGB, as revealed by defect-selective etching, which are known to consist of arrays of dislocations with a higher local density than surrounding regions. These hexagonal pits are similar to the so-called "V defects" previously observed in GaN, InGaN, and AlGaN epilayers. V defects in these materials are the result of crystalline faceting of the stable {10.1} planes during *c*-plane growth. Transmission electron microscopy studies of GaN and InGaN have shown that many, but not all, V defects are generated at the intersection of threading dislocations with the film surface. The correspondence between regions with high hexagonal pit density and regions with LAGB in our AlN films and substrates, respectively, suggests that the pits in the AlN films arise from a similar mechanism. The fact that some pits were arranged in well-defined linear arrays supports this assertion.

Frank[18] studied the capillary equilibrium of dislocations and formulated criteria for the morphology of a dislocation intersecting a crystal free surface, in effect establishing the conditions under which open pits, i.e., V defects, may be observed. This reduces to a competition between the crystal surface energy and the dislocation strain energy. Thus, surface pits may be made unstable by increasing the terrace width of steps on the growing crystal surface. This is achieved in practice by varying the Al supersaturation during AlN film growth, which can be achieved by varying the temperature, among other growth parameters.[14] Experiments were performed to determine if the V defects disappeared under different supersaturation conditions. Such a demonstration would indicate that opening of pits at threading dislocations intersecting the film free surface is an equilibrium phenomenon dependent on specific growth conditions. An AFM image of an AlN film grown under lower supersaturation conditions at 1250°C is shown in Fig. 4b. No pits of any size were observed in AFM, and optical microscopy was used to confirm that this was true for the entire film surface, indicating that a uniformly smooth film morphology, a necessary pre-requisite for device fabrication, was obtained by varying the supersaturation. Under these growth conditions it was not energetically favorable for dislocations intersecting the film free surface to form open pits. Additional experiments were performed to test the equilibrium conditions for pit opening. As described above, it had been observed that the pit diameter monotonically increased as a function of film thickness. Thus, films of a given thickness grown under similar supersaturation conditions favorable for pit opening contained pits of a characteristic size, while thicker films contained larger pits. Based on this observation, a 1 μm thick homoepi AlN film was grown under the conditions previously identified with no pit openings. Then the process parameters were changed to a higher supersaturation condition, previously identified with open pits, and an additional 1 μm was grown.

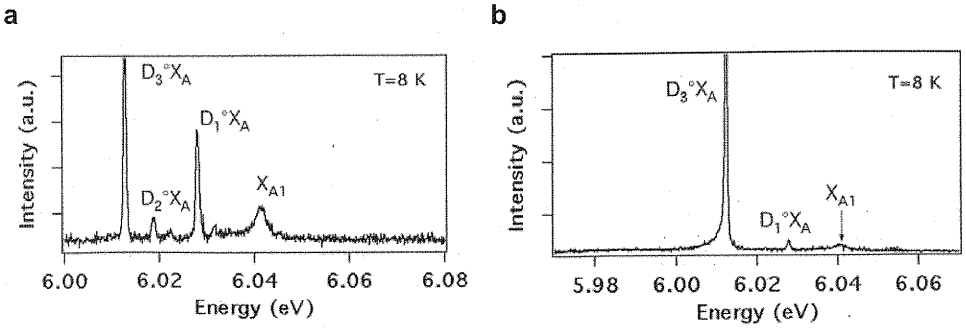

Figure 3. Low temperature near band edge PL spectra of AlN homoepitaxial films grown at (a) 1100°C and b) 1250°C, corresponding to [Si] of ~5×10^{16} and 2×10^{17} cm^{-3} in Figs. 2a and 2b, respectively.

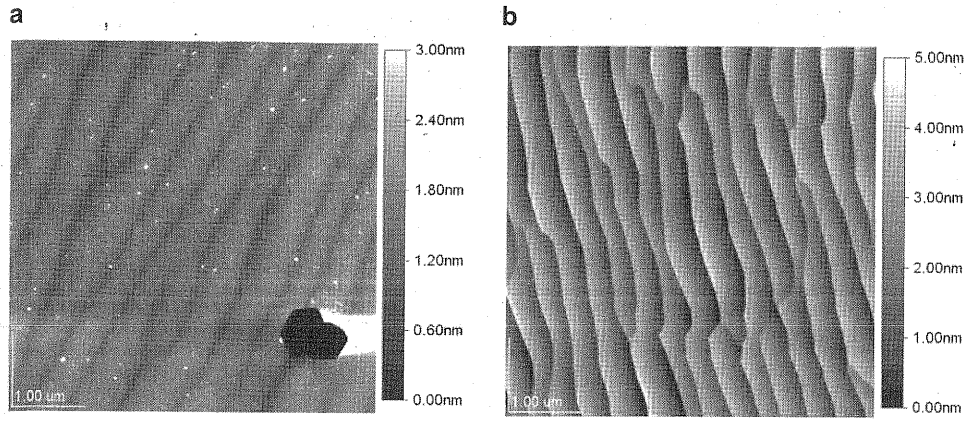

Figure 4. (Color online) (a) 5×5 μm^2 AFM image of a 2 μm thick AlN epilayer deposited at 1100°C on an AlN substrate oriented $< 1°$ off-axis from (00.1). A pair of 600 nm wide hexagonal pits are in contact with each other. (b) 5×5 μm^2 AFM image of a AlN epilayer deposited under lower Al supersaturation at 1250°C. No pits are visible in the AFM image. Film uniformity over the entire wafer surface was confirmed by optical microscopy.

When the as-grown surface was examined, pits with dimensions characteristic of a 1 μm thick film were observed, indicating that the dislocations threaded the entire film structure, but open pits were only produced when the equilibrium conditions favored their formation. These observations provide a useful guide for future growth of device layers with smooth surfaces.

AlGaN heteroepitaxy.—AlGaN films with Al compositions above 20% grown on GaN are typically cracked, due to the tensile in-plane strain. AlGaN grown on AlN is under compression, where buckling and cracking are the catastrophic failure modes providing relaxation. Dislocation nucleation and glide may also provide the necessary relaxation, but nitride materials possess a limited number of slip systems that are not easily activated. If relaxation is not necessary for a given application, films may be grown pseudomorphically, avoiding additional dislocation formation. AlGaN films of different thicknesses and compositions were grown on smooth AlN homoepitaxial layers, deposited on AlN substrates, in order to study relaxation in high Al content AlGaN. No cracking or buckling was observed in AlGaN films after growth.

Figure 5 shows triple axis ω-2θ scans for several AlGaN films. The reflections from the (00.2) planes of AlN and AlGaN were observed, along with Pendellösung thickness fringes around the AlGaN peaks for AlGaN films with compositions above 80% Al, which was attributed to the high quality of the films and heterointerfaces. In addition, the periodicity of the fringes was used to determine the AlGaN film thickness. Since the composition and relaxation of the AlGaN films cannot be uniquely determined from single ω-2θ scans,[19] they were determined by an x-ray diffraction method described in greater detail in Ref. 20. This method consisted of measuring the films' a and c lattice parameters from a series of relative asymmetric reflections in grazing incidence and grazing exit

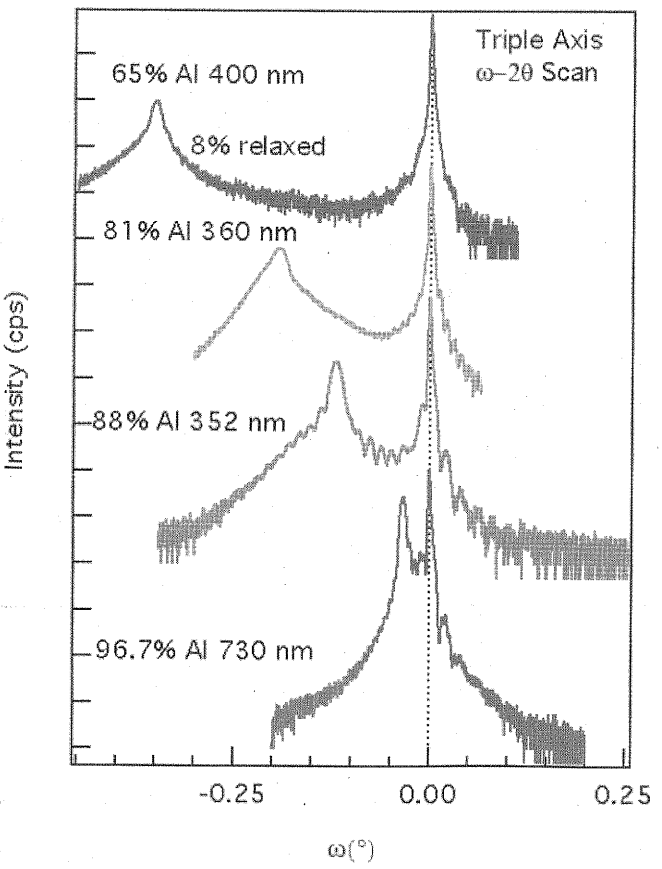

Figure 5. (Color online) Triple axis ω-2θ scans of AlGaN/AlN films grown on AlN substrates. The AlN (00.2) reflection is indicated by a dashed vertical line. Pendellösung thickness fringes are observed around the AlGaN peaks of AlGaN films with compositions above 80% Al.

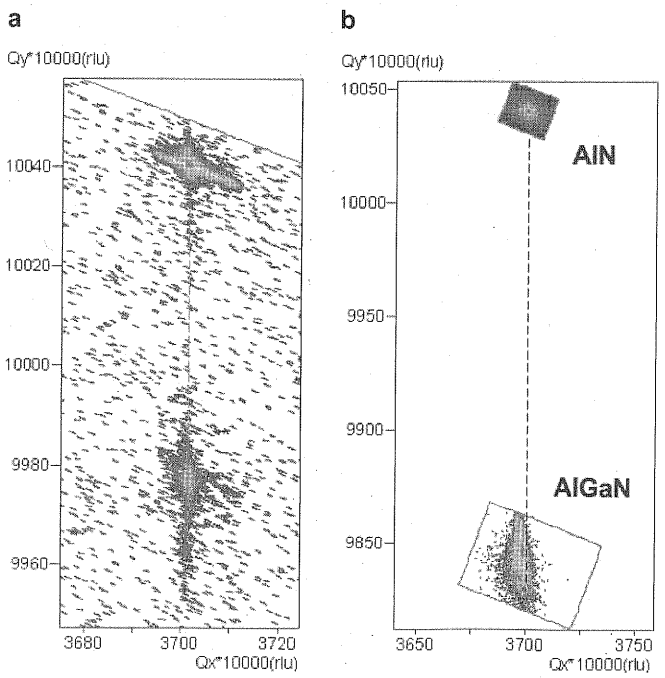

Figure 6. (Color online) RSMs of the asymmetric (10.5) reflections from (a) a 352 nm thick $Al_{0.88}Ga_{0.12}N$ film grown pseudomorphically on an AlN substrate, and (b) a 400 nm thick $Al_{0.65}Ga_{0.35}N$ film grown on AlN with 8% relaxation. The AlGaN RLP in (a) lies on a line that passes through the AlN RLP and is perpendicular to the Q_x axis, while in (b) the AlGaN RLP lies to the left of this line, corresponding to a larger a lattice parameter.

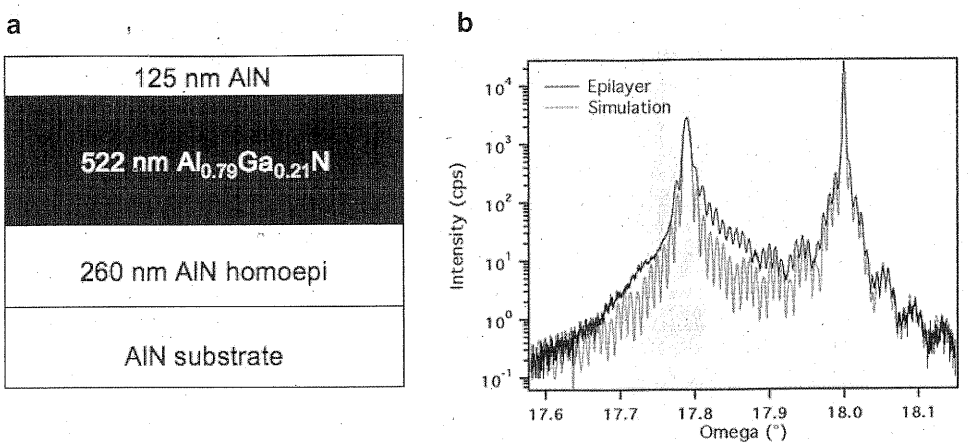

Figure 7. (a) Schematic drawing of the AlN/AlGaN/AlN epilayer structure deposited on an AlN substrate. The layer thicknesses and compositions were obtained from dynamical simulation of the experimental triple axis ω-2θ scan, shown in (b).

geometries, while confirming the values of the *c* lattice parameter from two complementary symmetric reflections. The strained AlGaN lattice parameters thus obtained were employed to determine the AlGaN composition and relaxation using elastic strain theory. The results of the various calculations are displayed in Fig. 5. Partial relaxation of 8% was observed for the 400 nm thick $Al_{0.65}Ga_{0.35}N$ film. This onset of relaxation was observed at a different Al composition than reported in Ref. 10. For compositions above 65% Al, the AlGaN films were pseudomorphic, that is, no relaxation was observed.

RSMs of the asymmetric (10.5) reflection were used to confirm the relaxation, obtained from the above-described method, of two of these films. Figure 6a shows the RSM of the un-relaxed AlGaN film with 88% Al content. A film is fully strained with respect to the underlying layer if the film's reciprocal lattice point (RLP) in an asymmetric RSM lies centered on a line that passes through the center of the RLP of the underlayer and is perpendicular to the Q_x axis.[19] In the case of AlGaN grown on *c*-plane AlN, this is equivalent to saying that the film and substrate have the same *a* lattice parameter, and corresponds to the relative position of the AlN and AlGaN RLPs observed in Fig. 6a. If this is not the case, the film is partially or fully relaxed. The RLP of a fully relaxed film lies on a line that joins the substrate RLP to the origin of the RSM. The AlGaN RLP in the RSM shown in Fig. 6b lies to the left of the vertical line that passes through the AlN RLP, indicating partial relaxation of the film, as was previously determined.

In order to further study the interfaces in AlN/AlGaN heterostructres, including the interface between the bulk substrate and the AlN homoepi film, an additional heterostructure was grown and analyzed by HRXRD and STEM. A schematic drawing of the thin film heterostructure is shown in Fig. 7a. It consisted of an AlGaN layer sandwiched between two AlN epilayers. The triple axis HRXRD ω-2θ scan, which probed the entire film structure including the substrate, is shown in Fig. 7b, where the reflections from AlGaN and AlN are seen at lower and higher angles, respectively. As in previous heterostructures analyzed by HRXRD, Pendellösung thickness fringes were observed in the scans, indicating the high quality and abruptness of the various interfaces. In addition to the experimental data, a dynamical simulation of the structure, showing good agreement with the experimental thickness fringes and main peak positions, is shown in the plot. Quantitative analysis of the simulation allowed us to extract the layer thicknesses and compositions, which are indicated in the schematic drawing in Fig. 7a. The experimental target Al composition for AlGaN was 80%, while x-ray analysis yielded 79%, indicating good process control. Analysis of the x-ray results also indicated that the AlGaN was coherent to AlN, i.e., a pseudomorphic layer was obtained.

A low magnification STEM image in Z-contrast mode, imaged along the [11–20] zone axis of the AlN/AlGaN/AlN heterostructure, is shown in Fig. 8a. Z-contrast is used to distinguish between regions of higher and lower average atomic number, resulting in brighter and darker contrast, respectively, in these regions. Turning to the image in Fig. 8a, one can see the upper and lower AlN epilayers surrounding the AlGaN, and a pair of thin layers at the sample surface (near the top of the image) exhibiting dark and light contrast. The thin layers at the sample surface are from C and Pt, dark and light contrast, respectively, deposited for FIB sample preparation. The AlGaN layer appears lighter than the surrounding AlN layers, due to Z-contrast, and its thickness agrees well with the value obtained from HRXRD. The interface between the AlN substrate and the AlN homoepi layer is indicated by an arrow. No dislocations are observed anywhere in the image. It should be noted that the sample foil that was prepared was approximately 6 μm wide, which is much larger that the image shown in Fig. 7a, and no dislocations were observed anywhere in the foil. Furthermore, the interface between the substrate and film had no distinguishable features associated with it. Its location was calibrated by using the film thicknesses obtained from HRXRD, but during STEM analysis, no interface-related features were observed. This indicates that the CMP process produced an epi-ready substrate surface with no subsurface damage, and that the *in-situ* nitridation used prior to film growth resulted in a surface free of oxides/hydroxides. Figure 8b shows a high magnification STEM image of the lower AlN/AlGaN epilayer interface. At this magnification, the image has a mottled appearance, due to roughening of the sample foil by FIB processing and possible

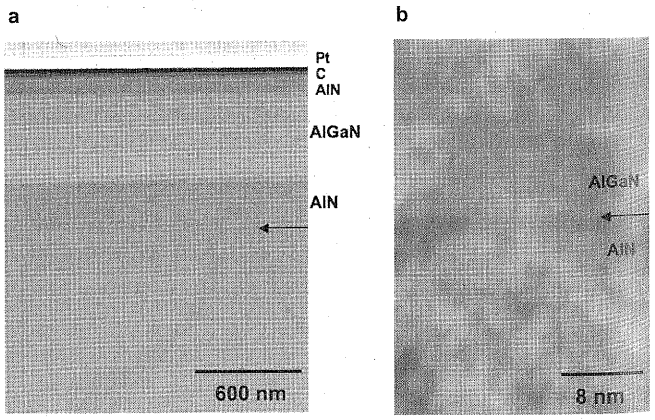

Figure 8. (a) Z-contrast STEM image of the AlN/AlGaN/AlN epilayer structure deposited on an AlN substrate. The AlGaN layer appears lighter due to its larger average atomic number. The location of the interface between the substrate and epilayer is indicated by an arrow. (b) High-magnification Z-contrast image of the lower AlN/AlGaN epilayer interface, with the location of the interface indicated by an arrow. Lattice fringes are clearly observed across the image, and the interface is abrupt, consistent with HRXRD characterization of this sample, Fig. 7b.

implantation damage from the Ga^+ ion beam. Clear lattice fringes and an atomically abrupt interface were observed, consistent with the observation of abrupt interfaces deduced from HRXRD. No additional misfit dislocations were observed at this interface, indicating the high-quality AlGaN layer was fully coherent to AlN. The upper AlN/AlGaN interface (not shown) was also imaged extensively, and the results were similar to those shown here.

Conclusions

High quality AlN homoepitaxy and AlGaN heteroepitaxy were demonstrated on single crystal AlN substrates. AlN films had low concentrations of background impurities, as determined by SIMS, resulting in well-defined excitonic emission near the band gap. Donor-bound exciton peaks with FWHM less than 0.5 meV were measured by PL. A HRXRD method based on relative measurements was used to determine the composition and relaxation of heteroepitaxial AlGaN films. Asymmetric RSMs confirmed partial relaxation of a 400 nm thick $Al_{0.65}Ga_{0.35}N$ film, while higher Al content films remained pseudomorphic. STEM analysis of an AlN/AlGaN/AlN epi heterostructure verified that CMP produced epi-ready substrate surfaces free of subsurface polishing damage, that high temperature substrate nitridation resulted in a clean surface suitable for epitaxy, and that high aluminum content AlGaN films with abrupt interfaces were grown pseudomorphically on AlN homoepitaxial films, without introduction of new strain-relieving dislocations.

Acknowledgments

This work was partially supported by NIST ATP grant no. 70NANB7H7045, Gerald Castellucci, project monitor; and by the Army Research Laboratory, contract no. W911QX-09-C-0002, Dr. Alfred Hung, program monitor.

HexaTech Inc. assisted in meeting the publication costs of this article.

References

1. Y. Taniyasu, M. Kasu, and T. Makimoto, *Nature*, **441**, 325 (2006).
2. R. Dalmau and Z. Sitar, in *Encyclopedia of Materials: Science and Technology*, K. H. J. Buschow, R. W. Cahn, M. C. Flemings, B. Ilschner, E. J. Kramer, S. Mahajan, and P. Veyssière, Editors, Updates, p. 1, Elsevier Science, Oxford (2008).
3. L. J. Schowalter, Y. Shusterman, R. Wang, I. Bhat, G. Arunmozhi, and G. A. Slack, *Appl. Phys. Lett.*, **76**, 985 (2000).
4. J. C. Rojo, L. J. Schowalter, R. Gaska, M. Shur, M. A. Khan, J. Yang, and D. D. Koleske, *J. Cryst. Growth*, **240**, 508 (2002).
5. S. A. Nikishin, B. A. Borisov, A. Chandolu, V. V. Kuryatkov, H. Temkin, M. Hotlz, E. N. Mokhov, Y. Makarov, and H. Helava, *Appl. Phys. Lett.*, **85**, 4355 (2004).
6. A. Sedhain, N. Nepal, M. L. Nakarmi, T. M. Al tahtamouni, J. Y. Lin, H. X. Jiang, Z. Gu, and J. H. Edgar, *Appl. Phys. Lett.*, **93**, 41905 (2008).
7. H. J. Kim, S. Choi, D. Yoo, J.-H. Ryou, R. D. Dupuis, R. F. Dalmau, P. Lu, and Z. Sitar, *Appl. Phys. Lett.*, **93**, 22103 (2008).
8. H. Helava, T. Chemekova, O. Avdeev, E. Mokhov, S. Nagalyuk, Y. Makarov, and M. Ramm, *Phys. Status Solidi C*, **7**, 2115 (2010).
9. Z. Ren, Q. Sun, S.-Y. Kwon, J. Han, K. Davitt, Y. K. Song, A. V. Nurmikko, H.-K. Cho, W. Liu, J. A. Smart, and L. J. Schowalter, *Appl. Phys. Lett.*, **91**, 51116 (2007).
10. J. R. Grandusky, J. A. Smart, M. C. Mendrick, L. J. Scowalter, K. X. Chen, and E. F. Schubert, *J. Cryst. Growth*, **311**, 2864 (2009).
11. R. Dalmau, R. Collazo, S. Mita, and Z. Sitar, *J. Electron. Mater.*, **36**, 414 (2007).
12. Z. G. Herro, D. Zhuang, R. Schlesser, R. Collazo, and Z. Sitar, *J. Cryst. Growth*, **286**, 205 (2006).
13. P. Lu, R. Collazo, R. F. Dalmau, G. Durkaya, N. Dietz, B. Raghothamachar, M. Dudley, and Z. Sitar, *J. Cryst. Growth*, **312**, 58 (2009).
14. A. Rice, R. Collazo, J. Tweedie, R. Dalmau, S. Mita, J. Xie, and Z. Sitar, *J. Appl. Phys.*, **108**, 43510 (2010).
15. R. A. R. Leute, M. Feneberg, R. Sauer, K. Thonke, S. B. Thapa, F. Scholz, Y. Taniyasu, and M. Kasu, *Appl. Phys. Lett.*, **95**, 31903 (2009).
16. T. Onuma, T. Shibata, K. Kosaka, K. Asai, S. Sumiya, M. Tanaka, T. Sota, A. Uedono, and S. F. Chichibu, *J. Appl. Phys.*, **105**, 23529 (2009).
17. L. Chen, B. J. Skromme, R. F. Dalmau, R. Schlesser, Z. Sitar, C. Chen, W. Sun, J. Yang, M. A. Khan, M. L. Nakarmi, J. Y. Lin, and H. X. Jiang, *Appl. Phys. Lett.*, **85**, 4334 (2004).
18. F. C. Frank, *Acta Crystallogr.*, **4**, 497 (1951).
19. M. A. Moram and M. E. Vickers, *Rep. Prog. Phys.*, **72**, 36502 (2009).
20. J. Tweedie, R. Collazo, A. Rice, J. Xie, S. Mita, R. Dalmau, and Z. Sitar, *J. Appl. Phys.*, **108**, 43526 (2010).